

Influence of superconducting gap structure on the quasiparticle spectrum in the vortex state

Masafumi Udagawa, Youichi Yanase, and Masao Ogata
Department of Physics, University of Tokyo, Hongo, Tokyo 113-0033, Japan
(Dated: November 13, 2018)

We study the vortex state of a layered superconductor with vertical line nodes on its Fermi surface when a magnetic field is applied in the ab-plane direction. We rotate the magnetic field within the plane, and analyze the change of low-energy excitation spectrum. Our analysis is based on the microscopic Bogoliubov-de Gennes equation and a convenient approximate analytical method developed by Pesch and Dahm. Both methods give a consistent result. Near the upper critical field H_{c2} , we observe a larger zero-energy density of states (ZEDOS) when the magnetic field is applied in the nodal direction, while much below H_{c2} , larger ZEDOS is observed under a field in the antinodal direction. We give a natural interpretation to this crossover behavior in terms of momentum distribution of low-energy quasiparticles. We examine the recent field angle variation experiments of thermal conductivity and specific heat. Comparison with our results suggest that special care should be taken to derive the position of line nodes from the experimental data. Combining the experimental data of the specific heat and our analyses, we conclude that Sr_2RuO_4 has vertical line nodes in the direction of the a-axis and the b-axis.

PACS numbers:

I. INTRODUCTION

Unconventional superconductors are one of the most important materials in the modern condensed matter physics, as a key to understanding strong electron correlation effect. A number of superconductors, high- T_c cuprates, heavy-fermion metals, ruthenates, and organic compounds exhibit unconventional behavior in the sense that the superconducting gap vanishes somewhere on the Fermi surface, resulting in power-law behaviors in various thermodynamic quantities. However, while many superconductors were found unconventional, detailed gap structures are still unexplored except for the cuprates. One of the difficulties in clarifying the gap structures seem to lie in the lack of experimental probes sensitive to quasiparticle momentum distribution.

Recently the vortex states have been attracting much interest, because the positions of gap nodes can be detected. When a magnetic field is applied parallel to the superconducting plane (ab-plane), various physical quantities depend on the angle between the magnetic field and the superconducting gap nodes. Hence, by rotating the field within the plane and tracing the change of physical quantities, one can obtain the information of the gap nodes. So far, thermal conductivity^{1,2,3,4,5,6,7,8,9} and specific heat^{10,11,12} have been measured in the vortex state for a number of layered unconventional superconductors including Sr_2RuO_4 ^{4,5,10}, CeCoIn_5 ^{6,11}, $\kappa\text{-(ET)}_2\text{Cu(NCS)}_2$ ⁷, $\text{YNi}_2\text{B}_2\text{C}$ ^{8,12} and $\text{PrOs}_4\text{Sb}_{12}$ ⁹.

However, it is found that some of these experiments show the behaviors incompatible with the results of

theoretical analyses. For example, microscopic calculations show an existence of vertical line nodes in Sr_2RuO_4 ^{13,14,15,16}, while the experiments suggest line nodes run horizontally^{4,5}. Probably these discrepancies are attributed to the lack of firm theoretical basis in analyzing the experimental data. Actually, experimental data have been interpreted based on a phenomenological Doppler-shift method, which has been claimed to be quite unreliable in some cases¹⁸. So far, there have been few microscopic analyses on quasiparticle states under a magnetic field parallel to the ab-plane. In particular, no microscopic analysis has been done on layered unconventional superconductors. Therefore, it is crucial to establish a reliable theory in these systems, and give a correct interpretation of the experiments.

In this paper, we present a detailed study of quasiparticle density of states in a layered superconductor under a magnetic field. We will focus on Sr_2RuO_4 , in which positions of the line nodes are still controversial. A cylindrical Fermi surface with vertical line nodes of f-wave symmetry is assumed, and a magnetic field is applied parallel to the ab-plane. We concentrate on the two cases where a magnetic field is in the nodal direction, and in the antinodal direction. We investigate the low-energy quasiparticle states, and apply the results to the interpretation of the experimental data.

Our analysis is based on the microscopic Bogoliubov de Gennes equation and an approximate analytical method invented by Pesch and recently developed by Dahm.

In the next section, calculational formulation is described. In section III, we will show our results and dis-

cussion on the experiments. Section IV contains conclusion.

II. FORMULATION

A. Model and Some features

First, we introduce some general features of our model. We study a quasi-two-dimensional layered superconductor which has a cylindrical Fermi surface with small c-axis dispersion. Thus we assume a dispersion relation,

$$\epsilon_{\mathbf{p}} = \frac{\mathbf{p}_{ab}^2}{2m_{ab}} - v_c \cos k_z, \quad (1)$$

where \mathbf{p}_{ab} is the momentum in the ab-plane and the c-axis wave number k_z varies in the interval $[-\pi, \pi]$. In this system, the Fermi velocity can be written in the following form,

$$\mathbf{v}_F = v_F(\cos \phi \mathbf{e}_a + \sin \phi \mathbf{e}_b + \epsilon \sin k_z \mathbf{e}_c), \quad (2)$$

with $v_F = \frac{P_F}{m_{ab}}$, and $v_c = \epsilon v_F$. Here, the azimuthal angle ϕ varies between $[0, 2\pi]$. The c-axis dispersion ϵ exists due to a small inter-layer hopping.

In this paper, we consider a spin-triplet superconducting order parameter with its \mathbf{d} -vector directed parallel to the c-axis

$$\hat{\Delta}(\mathbf{k}) = \begin{pmatrix} 0 & \Delta(\mathbf{k}) \\ \Delta(\mathbf{k}) & 0 \end{pmatrix}. \quad (3)$$

We fix the momentum part of the order parameter as

$$\Delta(\mathbf{k}) = \Delta_0(\hat{k}_a + i\hat{k}_b)(\hat{k}_a^2 - \hat{k}_b^2), \quad (4)$$

and ignore field-induced symmetry change of the order parameter. This is the simplest model of chiral state with four-fold symmetric vertical line nodes. In this model, nodes exist at $|\hat{k}_a| = |\hat{k}_b|$. However, exact positions of nodes are not important in the following discussion. Qualitative behavior of low-energy density of states is determined by the relation between applied field and line nodes.

In order to study the vortex state under a magnetic field parallel to the ab-plane, we assume a spatial variation of the order parameter, $\psi(\mathbf{r})\Delta(\mathbf{k})$. Here $\psi(\mathbf{r})$ is described by the Abrikosov vortex square lattice with anisotropic superconducting coherence lengths,

$$\psi(\mathbf{r}) = 2^{\frac{1}{4}} \sum_{n=-\infty}^{\infty} \exp\left(inq\frac{z}{\xi_c} - \frac{1}{2}\left(\frac{r_{\perp}}{\xi_{ab}} - nq\right)^2\right), \quad (5)$$

where, ξ_c and ξ_{ab} are the superconducting coherence lengths in the c-axis and the ab-plane directions, respectively, and r_{\perp} denotes the coordinate for an axis which is in the ab-plane and is perpendicular to the magnetic field. For example, $\psi(\mathbf{r})$ is equal to zero at the position

$r_{\perp} = \frac{q}{2}\xi_{ab}$ and $z = \frac{\pi}{q}\xi_c$, representing the center of a vortex. In eq. (5), the prefactor $2^{\frac{1}{4}}$ is a normalization factor to let the cell average of $|\psi(\mathbf{r})|^2$ equal to 1. We have adopted the Landau gauge for the vector potential as

$$\mathbf{A}(\mathbf{r}) = Br_{\perp}\mathbf{e}_c. \quad (6)$$

It is apparent that $\psi(\mathbf{r})$ has a periodicity with respect to \mathbf{r} , which corresponds to the vortex unit cell. The spatial periods L_c (c-axis direction) and L_{ab} (ab-plane direction) are related to q as

$$L_{ab} = q\xi_{ab}, \quad (7)$$

$$L_c = \frac{2\pi\xi_c}{q}. \quad (8)$$

We choose q so that the ratio $\frac{L_{ab}}{L_c}$ is equal to $\frac{\xi_{ab}}{\xi_c}$ in the whole range of magnetic field. Then, $\psi(\mathbf{r})$ can be rewritten as

$$\psi(\mathbf{r}) = 2^{\frac{1}{4}} \sum_{n=-\infty}^{\infty} \exp\left(2i\pi n\frac{z}{L_c} - \pi\left(\frac{r_{\perp}}{L_{ab}} - n\right)^2\right). \quad (9)$$

Since the size of a vortex unit cell is inversely proportional to the average induction B , we have the following relation

$$L_j(B) = \sqrt{2\pi}\xi_j\sqrt{\frac{B_{c2}}{B}} \quad (j = c, ab). \quad (10)$$

Finally, we introduce parameters and physical quantities of interest. Most properties in our system are determined by a single parameter, namely the reduced order parameter $\eta(B)$ defined by

$$\eta(B) = \sqrt{\frac{2}{\pi}} \frac{\Delta_0(B)L_{ab}(B)}{v_F}, \quad (11)$$

where $\Delta_0(B)$ is a spatial average of the order parameter. Note that η monotonically decreases as increasing magnetic field H and becomes 0 when H reaches H_{c2} .

We are interested in how the density of states(DOS) depend on the angle α between the field and the line node when a field rotates within the plane. It is expected that the density of states oscillates with the period $\frac{\pi}{2}$, reflecting the fourfold symmetry of the order parameter. Therefore, we can concentrate on the two cases: when a field is applied in the nodal direction($\alpha = 0$), and in the antinodal direction ($\alpha = \pi/4$). DOS is considered to take its minimum and maximum in one and the other of these two cases, respectively.

B. Bogoliubov-de Gennes equation

Using above dispersion relations and spatially inhomogeneous superconducting order parameter, we solve the

Bogoliubov-de Gennes(BdG) equation, which is considered to be the most reliable approach²¹.

$$\hat{H}_0 u_\sigma(\mathbf{r}) + \hat{\Delta}(-i\nabla) \left[\psi \left(\frac{\mathbf{r} + \mathbf{r}'}{2} \right) v_\sigma(\mathbf{r}) \right] \Big|_{\mathbf{r}' \rightarrow \mathbf{r}} = E u_\sigma(\mathbf{r}), \quad (12)$$

$$- \hat{\Delta}^*(i\nabla) \left[\psi^* \left(\frac{\mathbf{r} + \mathbf{r}'}{2} \right) u_\sigma(\mathbf{r}) \right] \Big|_{\mathbf{r}' \rightarrow \mathbf{r}} - \hat{H}_0^* v_\sigma(\mathbf{r}) = E v_\sigma(\mathbf{r}), \quad (13)$$

where

$$\hat{H}_0 = \frac{1}{2m_{ab}} \left(\mathbf{P}_{ab} - \frac{e}{c} \mathbf{A} \right)^2. \quad (14)$$

Here we assumed $\epsilon \ll 1$, and neglected the effect of the c-axis dispersion. This prescription corresponds to neglecting a coherence along the c-axis direction, or in the quasiclassical sense, to taking account of only the trajectories parallel to the ab-plane. We will discuss the details of this prescription later in the next section. Eq. (12) and (13) can be decoupled into 2×2 matrix equation for $(u_\uparrow, v_\downarrow)$ and $(u_\downarrow, v_\uparrow)$. Since both the pairs satisfy the same equation, we can work on only one of them, say, $(u_\uparrow, v_\downarrow)$.

We numerically diagonalize Eqs. (11) and (12) by discretizing the coordinate \mathbf{r} , and obtain sets of eigenvalues E_K and eigenfunctions $(u_K(\mathbf{r}), v_K(\mathbf{r}))$. Using the obtained eigenfunctions, we calculate DOS $\nu_{BdG}(\epsilon)$:

$$\nu_{BdG}(\epsilon) = \sum_{E_K > 0} \int d\mathbf{r} [|u_K(\mathbf{r})|^2 \delta(\epsilon - E_K) + |v_K(\mathbf{r})|^2 \delta(\epsilon + E_K)]. \quad (15)$$

Due to the translational symmetry along the magnetic field, momentum parallel to the vortices, p_\parallel , becomes a good quantum number. Hence, for each eigenfunction, we can define an angle between the magnetic field and quasiparticle momentum as

$$\theta = \arctan \left(\frac{\sqrt{p_F^2 - p_\parallel^2}}{p_\parallel} \right) \quad (0 \leq \theta \leq \pi), \quad (16)$$

where we limit the range of θ to $[0, \pi]$ due to the reflectional symmetry about the magnetic field. Since momentum normal to the magnetic field p_\perp is not a conserved quantity, p_\perp has a finite width δp_\perp for each eigenstate. Nevertheless, $\frac{\delta p_\perp}{p_\perp}$ is much smaller than 1 (of the order of $\frac{1}{k_F \xi_{ab}}$), not too much below T_c . Therefore, we can consider θ as a well-defined quantity in the quasiclassical meaning. Using this θ , we discuss the momentum distribution of the quasiparticles contributing to zero-energy density of states.

C. Approximation due to Pesch and Dahm

Before showing our results of BdG equations, let us introduce an approximate analytical method, invented by Pesch¹⁷, and developed by Dahm^{18?}. We will compare the obtained results with this approximation. Near H_{c2} , spatial variation of order parameter is small. Hence, in the Eilenberger equations, it is allowed to replace normal component of quasiclassical Green functions g by its spatial average over a vortex unit cell. With this averaged quasiclassical Green function, we can calculate various observable quantities (e.g. DOS) in the averaged form over a vortex unit cell. According to Dahm¹⁸, even much below H_{c2} , this approximation gives the result quantitatively in agreement with that from the rigorous Eilenberger equation.

Here, we summarize the main results of this method. For details, see Ref.18. We assume that a spatial variation of the order parameter is described by $\psi(\mathbf{r})$, Abrikosov vortex lattice introduced in the section IIA. Then, the averaged density of states $\nu_{PD}(\epsilon)$ (in the unit of DOS for the normal state ν_0) can be written in the following form,

$$\nu_{PD}(\epsilon) = \left\langle \text{Re} \frac{1}{\sqrt{1 + P(\mathbf{v}_F, i\omega_n \rightarrow \epsilon + i0)}} \right\rangle_F, \quad (17)$$

where $\langle \dots \rangle_F$ means averaging on the Fermi surface, and in our system, $P(\mathbf{v}_F, i\omega_n)$ is written as

$$P(\mathbf{v}_F, i\omega_n) = \frac{4|\Delta(\mathbf{k})|^2}{\pi|\mathbf{v}_{F\perp}|^2} \left[1 - \frac{\sqrt{2}\omega_n}{|\mathbf{v}_{F\perp}|} e^{\frac{2\omega_n^2}{\pi|\mathbf{v}_{F\perp}|^2}} \times \text{erfc} \left(\frac{\sqrt{2}\omega_n}{\sqrt{\pi}|\mathbf{v}_{F\perp}|} \right) \right], \quad (18)$$

where $\mathbf{v}_{F\perp}$ is the projection of the scaled Fermi velocity onto the plane normal to the magnetic field,

$$\mathbf{v}_{F\perp} = v_F \left(\frac{\cos \theta}{\xi_{ab}} \mathbf{e}_{ab} + \frac{\epsilon \sin k_z}{\xi_c} \mathbf{e}_c \right). \quad (19)$$

The momentum distribution of zero-energy quasiparticles is simply given by

$$\nu_{PD}(0, \mathbf{v}_F) = \text{Re} \frac{1}{\sqrt{1 + P(\mathbf{v}_F, i\omega_n \rightarrow +i0)}}. \quad (20)$$

III. RESULTS

A. Zero-energy density of states(ZEDOS)

First, we will discuss the density of states right at zero-energy. In Fig. 1, we show our results for the η dependence of ZEDOS $\frac{\nu_j(0)}{\nu_0}$ for $j = n, a$, calculated with the BdG and the PD methods. ZEDOS under a field in the nodal direction ($\alpha = 0$) is denoted as $\nu_n(0)$ and in the anti-nodal direction ($\alpha = \frac{\pi}{4}$) as $\nu_a(0)$. Both $\nu_n(0)$ and $\nu_a(0)$ are normalized to the normal-state value.

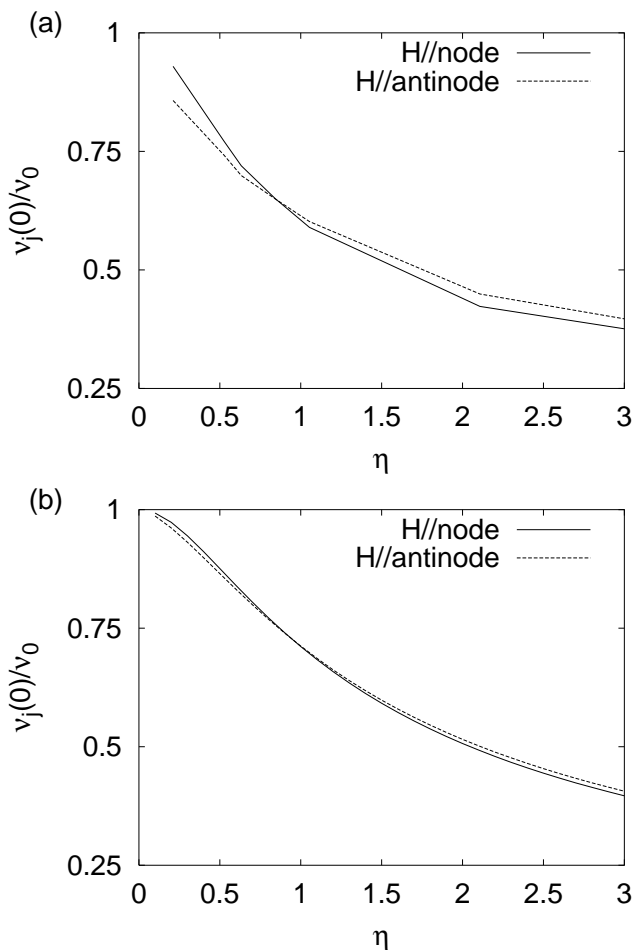


FIG. 1: The η dependence of zero-energy density of states calculated with (a) the BdG method and (b) the PD method. The solid line shows ZEDOS for $\mathbf{H} \parallel \text{node} (\alpha = 0)$, i.e. $\frac{\nu_n(0)}{\nu_0}$, while the dashed line shows ZEDOS for $\mathbf{H} \parallel \text{antinode} (\alpha = \frac{\pi}{4})$, i.e. $\frac{\nu_a(0)}{\nu_0}$. ZEDOS is normalized to the normal-state value.

Two results show a similar behavior that in a high magnetic field or when \mathbf{H} is close to H_{c2} (low η), $\nu_n(0) > \nu_a(0)$, while in a low magnetic field (high η), $\nu_a(0) > \nu_n(0)$.

In order to understand this crossover behavior, let us see the momentum distribution of quasiparticles contributing to the zero-energy density of states. Figure 2 shows the angle-resolved ZEDOS obtained with the BdG method for several values of η . In a low field region (Fig. 2(a)), it is found that narrow regions in Fermi surface are responsible for ZEDOS. In the case of $\mathbf{H} \parallel \text{node} (\alpha = 0)$, a sharp peak appears at $\theta = 90^\circ$ which corresponds to the nodal direction perpendicular to the magnetic field. In contrast, the nodal quasiparticles running parallel to the field ($\theta = 0^\circ, 180^\circ$) give much smaller contribution to ZEDOS. In the case of $\mathbf{H} \parallel \text{antinode} (\alpha = \frac{\pi}{4})$, we can observe nodal peaks of the same height at $\theta = 45^\circ$ and 135° .

With increasing magnetic field (decreasing η) (Fig. 2(b)), nodal peaks become broader, and the contribution from the core states increases by a large amount, commonly for both α . This is because the decrease of order parameter amplitude makes it easier for low-energy quasiparticles to propagate independent of α . However, as for the quasi-particles running parallel to the field (i.e. $\theta = 0^\circ, 180^\circ$), we can see a big difference between the two cases. In the case of $\mathbf{H} \parallel \text{node}$, contribution from the field direction becomes larger with increasing field strength, while in the case of $\mathbf{H} \parallel \text{antinode}$, contribution from this direction remains small.

When the field strength is increased (η is decreased) further (Fig. 2(c)), nodal peaks become too broad to be identified. In most part of the Fermi surface, the angle-resolved ZEDOS recover the normal-state value. Nevertheless, appreciable difference still exists for the quasiparticles running parallel to the field.

We can understand the nature of this difference by using the idea of quasi-classical trajectories. In the quasi-classical theory, a trajectory is determined from the Fermi velocity and an impact parameter. ZEDOS can be obtained by summing over contributions from those trajectories. Roughly saying, if the sign of order parameter changes on a trajectory, finite contribution to ZEDOS arises due to the formation of Andreev bound states. Now let us consider the trajectories parallel to the field. In the case of $\mathbf{H} \parallel \text{node}$, quasiparticles propagating along such trajectories feel no superconducting gap due to the gap node irrespective of impact parameter. On the other hand, in the case of $\mathbf{H} \parallel \text{antinode}$, those quasiparticles feel finite and spatially uniform gap, because they propagate along the vortices and never cross vortex cores. (Only part of the quasiparticles run right through a vortex core and feel no superconducting gap. However, contributions from such trajectories are considerably small.) Hence, in the latter case, those quasiparticles are hampered by finite and uniform order parameter and cannot contribute to ZEDOS, no matter how small (high) order parameter amplitude (magnetic field) is. This is why ZE-

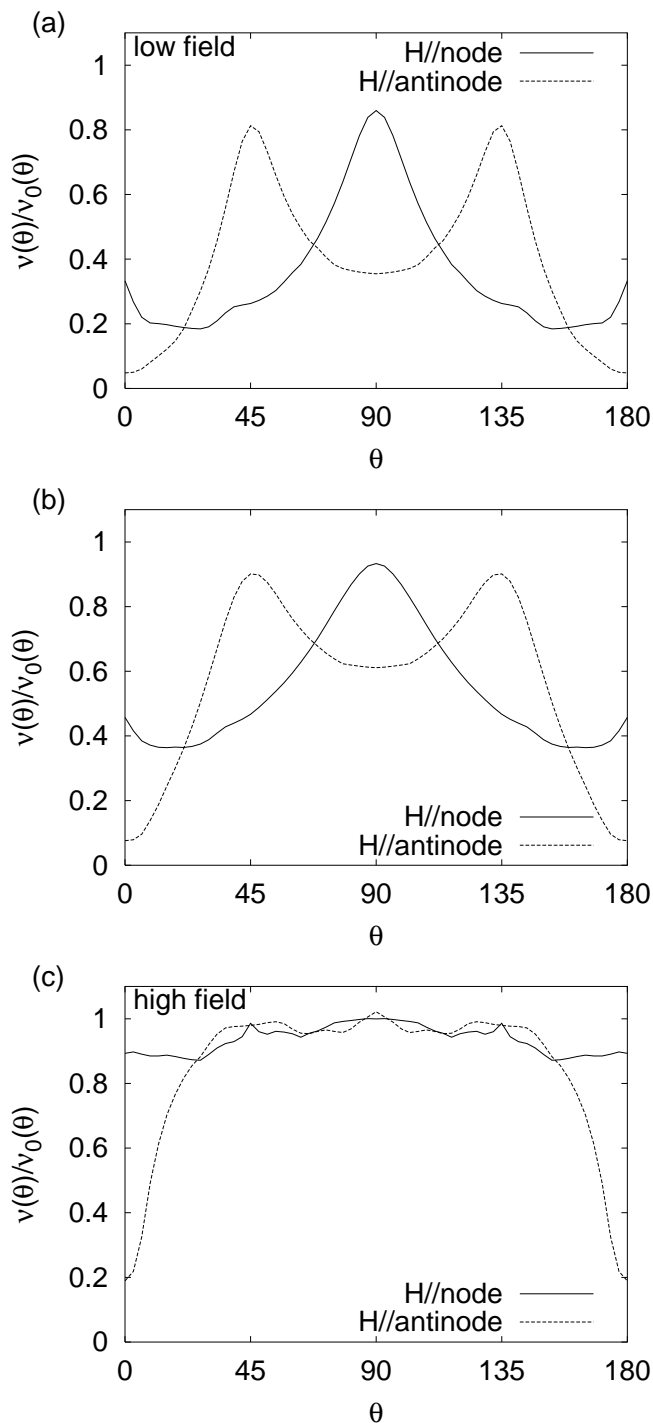


FIG. 2: Angle-resolved ZEDOS(normalized to the normal-state value) calculated with the BdG method. θ is measured from the field direction. (a) $\eta = 2.11$, (b) $\eta = 1.05$, and (c) $\eta = 0.21$

DOS is suppressed in the case of $\mathbf{H} \parallel$ antinode in a high magnetic field region.

Next, let us compare the above results with the angle-resolved ZEDOS derived from the PD method (Fig. 3) by integrating Eq.(20) with respect to k_z . In most part

of the Fermi surface, we observe much the same behavior as the BdG results. However, as for the quasiparticles running in the field direction($\theta = 0^\circ, 180^\circ$), the PD method gives larger angle-resolved ZEDOS than that in BdG method. We attribute this difference to the prescription we made in solving the BdG equations, that is, a neglect of c-axis dispersion term. This prescription corresponds to considering only the trajectories parallel to the ab-plane, i.e. limiting the c-axis component of the Fermi velocity k_z to 0. Hence, our prescription enhances the contribution of the quasiparticles propagating in the direction ($\theta = 0, k_z = 0$) compared with other contributions of $k_z \neq 0$ quasiparticles. As we have discussed above, it is those quasiparticles with $k_z = 0$ that suppress ZEDOS in the case $\alpha = \frac{\pi}{4}$. Therefore, we obtain smaller angle-resolved ZEDOS from the BdG method. For comparison, we plot the angle-resolved ZEDOS obtained from Eq. (20) with $k_z = 0$ in Fig. 4. Comparing it with Fig. 2(a), a quantitative agreement can be seen in $\theta \sim 0^\circ$ and 180° .

Further, we comment on the difference in ZEDOS observed in a high magnetic field region($\eta \sim 0.1$) between Figs. 1(a) and (b). Since the behavior of ZEDOS in this magnetic field region is dominated by the quasiparticles parallel to the field, our BdG analysis overestimates the difference in ZEDOS.

Here we briefly summarize the main results in this subsection. In a low magnetic field region, ZEDOS is dominated by nodal quasiparticles which have a finite momentum normal to the field. In this region, we have $\nu_a(0) > \nu_n(0)$, since in the case of $\mathbf{H} \parallel$ node, two of the four nodes are parallel to the field, thus unable to contribute to ZEDOS, while in the case of $\mathbf{H} \parallel$ antinode, all the four nodes can contribute to ZEDOS. In a high magnetic field region, on the other hand, the difference between $\nu_a(0)$ and $\nu_n(0)$ comes from the behavior of quasiparticles running in the field direction. In the case of $\mathbf{H} \parallel$ antinode, those quasiparticles are hampered by finite and uniform order parameter and cannot contribute to ZEDOS, while in the case of $\mathbf{H} \parallel$ node, they can. Therefore, we have $\nu_n(0) > \nu_a(0)$ in this field region.

B. Density of states(DOS)

Next, we will show our results for the density of states at finite energy. DOS at finite energy is particularly important when we discuss the experimental data, because it depends on the density of states at $0 \lesssim \epsilon \lesssim k_B T$. In Figs. 5 and 6, we show DOS obtained with the BdG and the PD methods, respectively.

Let us first discuss the high magnetic field region (Figs. 5(b) and 6(b)). We can observe a sharp rise in DOS at $|\epsilon| \sim \Delta_0$ reminiscent of a coherence peak in the case of $\mathbf{H} \parallel$ antinode, while not in the case of $\mathbf{H} \parallel$ node. This

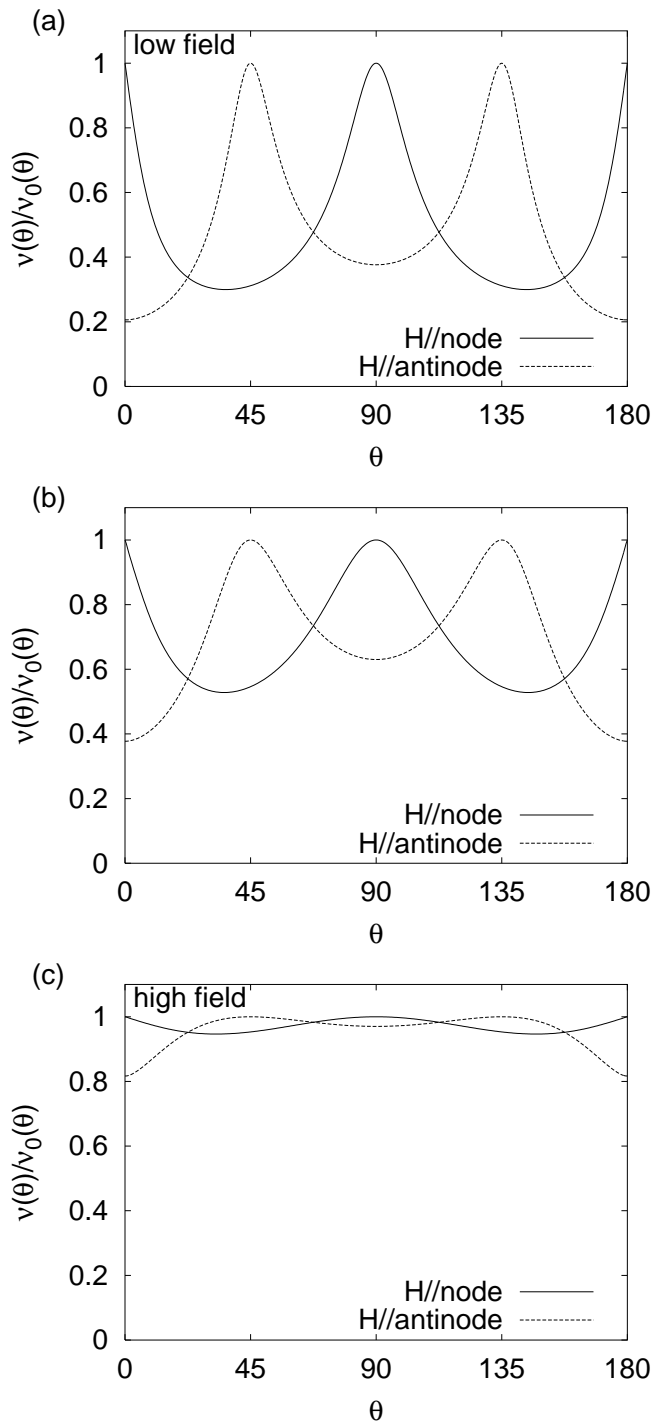


FIG. 3: Angle-resolved ZEDOS(normalized to the normal-state value) calculated with the PD method. θ is measured from the field direction. (a) $\eta = 2.11$, (b) $\eta = 1.05$, and (c) $\eta = 0.21$.

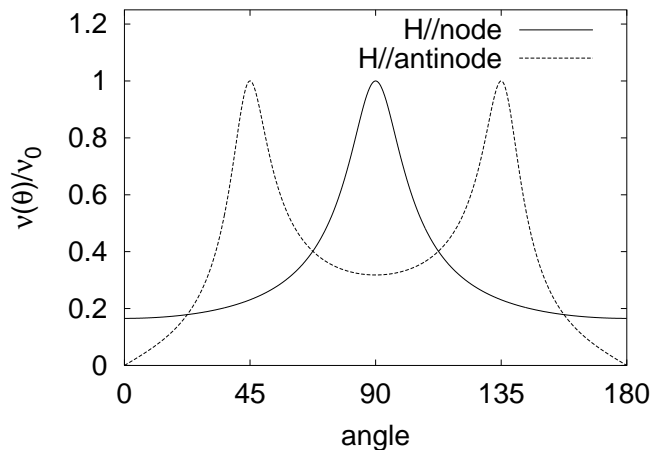


FIG. 4: Angle-resolved ZEDOS(normalized to the normal-state value) calculated with the PD method with $k_z = 0$ for $\eta = 2.11$.

character of DOS reflects the behavior of the quasiparticles running parallel to the field. Since they feel finite order parameter in the case of $\mathbf{H} \parallel$ antinode, they tend to form a coherence peak. This coherence-peak like structure appears more clearly in the BdG result due to our prescription as discussed in the previous subsection.

In this high magnetic field region, we observe $\nu_n(\epsilon) > \nu_a(\epsilon)$ for $0 \lesssim |\epsilon| \lesssim \Delta_0$ independent of the calculational methods. Therefore, if the thermal conductivity or the specific heat is measured in this field region with a rotating magnetic field, maximum will be observed when the field is applied in the nodal direction.

The results for a low magnetic field region are shown in Fig. 5(a) and 6(a). In this field region, as we have discussed in the previous subsection, $\nu_a(0) > \nu_n(0)$ at zero-energy. However, as shown in Fig. 5(a) and 6(a), $\nu_a(\epsilon)$ and $\nu_n(\epsilon)$ cross at $|\epsilon| \sim 0.2\Delta_0$. For $|\epsilon| > 0.2\Delta_0$ we have the opposite inequality $\nu_n(\epsilon) > \nu_a(\epsilon)$. This means that when we take experimental data at a temperature $T \gtrsim 0.2\Delta_0$ with a rotating magnetic field within the plane, we will observe very small angle variation, because the effects of lower-energy DOS and higher-energy DOS cancel each other.

C. Interpretations of the experimental data

In this subsection, we will discuss how to interpret the experimental data of the thermal conductivity and the specific heat, in connection with our analyses.

So far the thermal conductivity^{4,5} and the specific heat¹⁰ of Sr_2RuO_4 have been measured under a rotating in-plane field by several groups. In the experiments of the magnetothermal conductivity, they found no angle variation, except in the vicinity of H_{c2} . They attributed the angle variation near H_{c2} to the anisotropy of H_{c2} itself, and denied the existence of vertical line nodes in

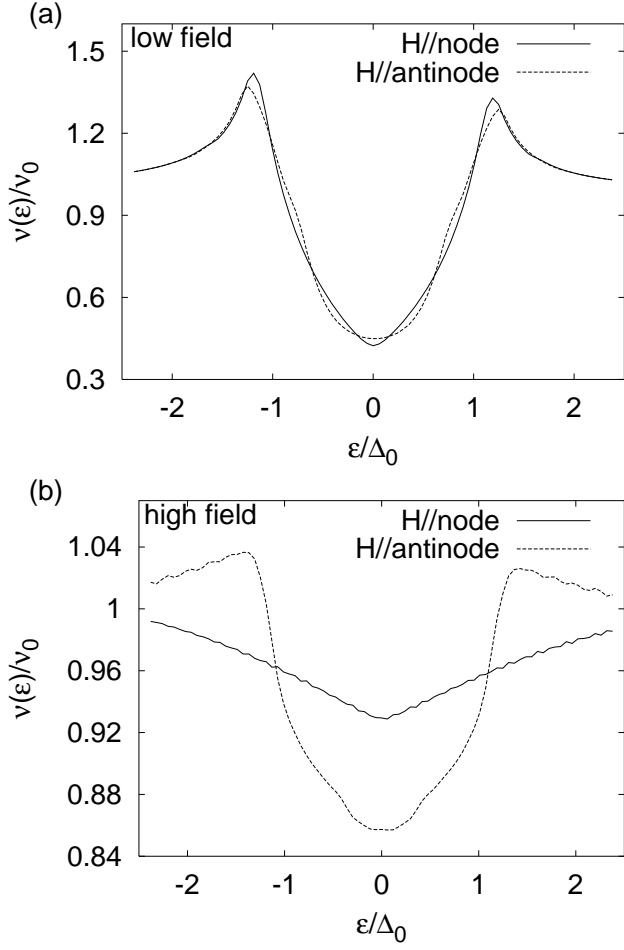


FIG. 5: Finite-energy DOS(normalized to the normal-state value) calculated with the BdG method. (a) $\eta = 2.11$ and (b) $\eta = 0.21$.

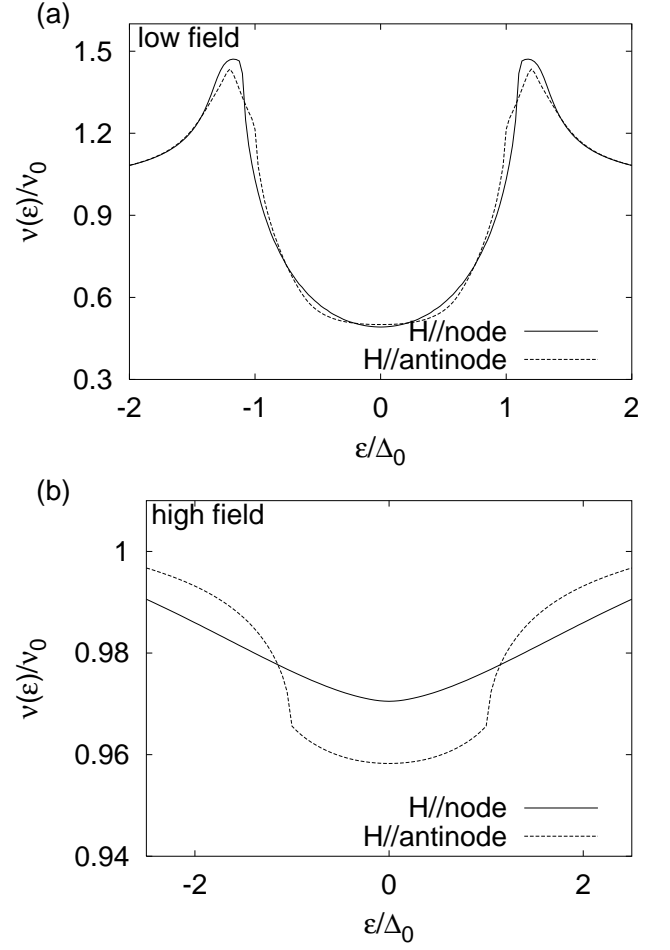


FIG. 6: Finite-energy DOS(normalized to the normal-state value) calculated with the PD method. (a) $\eta = 2.11$ and (b) $\eta = 0.21$.

Sr_2RuO_4 . On the other hand, in the experiment of the specific heat, fourfold oscillation is found at a lower field, in addition to the angle variation near H_{c2} . For the angle variation at the lower field, the specific heat shows maximum at $\mathbf{H}||[110]$, while near H_{c2} maximum is observed at $\mathbf{H}||[100]$. These measurements seem to provide incompatible results. However, our theoretical analysis gives an answer to this contradiction in the following way.

Here we discuss why the thermal conductivity does not show the fourfold oscillation in the low field region. As we show in the previous subsection, the reversal of $\nu_n(\epsilon)$ and $\nu_a(\epsilon)$ occurs in this field region at $\epsilon \sim 0.2\Delta_0$. Thus, in order to observe the anisotropy of ZEDOS in this field region, contribution from higher energy part of DOS must be removed. However, the thermal conductivity is measured at rather high temperatures $T = 0.2 - 0.3T_c$, where the effect of high energy part of DOS mixes inevitably as we note in the previous subsection. Hence, it is no wonder that the anisotropy of ZEDOS cannot be observed. On the other hand, the measurement of the specific heat was conducted at a lower temperature $T < 0.1T_c$, where the

specific heat is sensitive to ZEDOS. Furthermore, note that the specific heat is more sensitive to the low energy part of DOS than the thermal conductivity. These will be the reason why they can observe the fourfold oscillation.

Combining the above considerations, we can determine the position of line nodes. In the measurement of the specific heat, the maximum was found at $\mathbf{H}||[110]$, while from our calculations we have $\nu_a(0) > \nu_n(0)$ in a low magnetic field region. Therefore, we conclude that the line nodes exist in the direction $[\pm 100]$ and $[0\pm 10]$.

In sections IIIA and IIIB, we have shown that $\nu_n(\epsilon) > \nu_a(\epsilon)$ for $0 \lesssim |\epsilon| \lesssim \Delta_0$ in a high magnetic field region. Therefore, in this field region, there is a possibility that we can observe a fourfold oscillation both in the thermal conductivity and the specific heat, aside from the effect of the anisotropy in H_{c2} .

In summary, we can explain the data of specific heat and thermal conductivity simultaneously by assuming the vertical line nodes along $[\pm 100]$ axis. The line nodes in this direction is expected in the γ -band from the relation between the Fermi surface and crystal symmetry

(Ref.14), and has been confirmed in microscopic analysis (Ref.15). Strictly speaking, these are not line nodes, because excitation gap is small but finite. However, tiny gaps serve as line nodes in the finite temperature.

IV. CONCLUSIONS

We studied the density of states in the vortex state of a layered superconductor with vertical line nodes on the cylindrical Fermi surface under a field parallel to the ab-plane. We investigated the angle variation of DOS with changing field strength. Bogoliubov-de Gennes equation and an approximate analytical method due to Pesch and Dahm were solved. We found that a field in the nodal direction gives larger zero-energy density of states in a higher magnetic field region, whereas a field in the anti-nodal direction results in larger zero-energy density of states in a lower magnetic field region. This crossover phenomenon is naturally understood in terms of the momentum distribution of quasiparticles. In a higher field region, under a field applied in the anti-nodal direction, quasiparticles running parallel to the field is hampered

by spatially uniform order parameter, and thus gives a smaller contribution to ZEDOS compared with the case in which the field is applied in other directions. In a lower field region, nodal quasiparticles not parallel to the field contribute to ZEDOS significantly. Therefore, when the field is applied in the anti-nodal direction, four such nodes are available, which leads to the larger ZEDOS compared with the case of $\mathbf{H} \parallel$ node, where only two such nodes are available.

We investigated the angle variation of the density of states at finite energy. We found that in a low magnetic field region, DOS at $\epsilon \gtrsim 0.2\Delta_0$ shows maximum when the field is parallel to the node, while ZEDOS shows minimum for this field direction. On the basis of this fine structure of DOS, we discussed why the thermal conductivity does not show fourfold oscillation in the low field region. Finally, combining the experimental data of the specific heat and our analyses, we conclude that Sr_2RuO_4 has vertical line nodes in the direction of the a-axis and the b-axis.

We are grateful to K. Deguchi for teaching us his experimental results. we also thank N. Yoshida for helpful discussions.

-
- ¹ F. Yu, M. B. Salamon, A. J. Leggett, W. C. Lee, and D. M. Ginsberg, Phys. Rev. Lett **74**, 5136 (1995).
² H. Aubin, K. Behnia, M. Ribault, R. Gagnon, and L. Taillefer, Phys. Rev. Lett **78**, 2624 (1997).
³ R. Ocaña and P. Esquinazi, Phys. Rev. Lett **87**, 167006-1 (2001).
⁴ K. Izawa, H. Takahashi, H. Yamaguchi, Yuji Matsuda, M. Suzuki, T. Sasaki, T. Fukase, Y. Yoshida, R. Settai, and Y. Onuki, Phys. Rev. Lett **86**, 2653 (2001).
⁵ M. A. Tanatar, M. Suzuki, S. Nagai, Z. Q. Mao, Y. Maeno, and T. Ishiguro, Phys. Rev. Lett **86**, 2649 (2001).
⁶ K. Izawa, H. Yamaguchi, Yuji Matsuda, H. Shishido, R. Settai, and Y. Onuki, Phys. Rev. Lett **87**, 057002 (2001).
⁷ K. Izawa, H. Yamaguchi, T. Sasaki, and Yuji Matsuda, Phys. Rev. Lett **88**, 027002 (2002).
⁸ K. Izawa, K. Kamata, Y. Nakajima, Y. Matsuda, T. Watanabe, M. Nohara, H. Takagi, P. Thalmeier, and K. Maki Phys. Rev. Lett **89**, 137006 (2002).
⁹ K. Izawa, Y. Nakajima, J. Goryo, Y. Matsuda, S. Osaki, H. Sugawara, H. Sato, P. Thalmeier, and K. Maki Phys. Rev. Lett **90**, 117001 (2003).
¹⁰ K. Deguchi, Z. Q. Mao, H. Yaguchi, and Y. Maeno, cond-mat/0311366.
¹¹ H. Aoki, T. Sakakibara, H. Shishido, R. Settai, Y. Onuki, P. Miranović, and K. Machida, cond-mat/0312012
¹² Tuson Park, M. B. Salamon, Eun Mi Choi, Heon Jung Kim, and Sung-Ik Lee Phys. Rev. Lett **90**, 177001 (2003).
¹³ K. Kuroki, M. Ogata, R. Arita and H. Aoki, Phys. Rev. B **63**, 060506(R) (2001).
¹⁴ K. Miyake and O. Narikiyo, Phys. Rev. Lett **83**, 1423 (1999).
¹⁵ T. Nomura and K. Yamada, J. Phys. Soc. Jpn. **71**, 404 (2002).
¹⁶ M. J. Graf and A. V. Balatsky, Phys. Rev. B **62**, 9697 (2002).
¹⁷ W. Pesch, Z. Phys. B **21**, 263 (1975); P. Klimesch and W. Pesch, J. Low Temp. Phys. **32**, 869 (1978).
¹⁸ T. Dahm, S. Graser, C. Iniotakis, and N. Schopohl, Phys. Rev. B **66**, 144515 (2002).
¹⁹ S. Graser, T. Dahm, and N. Schopohl, cond-mat/0309142.
²⁰ P. Miranović, N. Nakai, M. Ichioka, and K. Machida, Phys. Rev. B **68**, 052501 (2003).
²¹ P. G. de Gennes, *Superconductivity of Metals and Alloys*.
²² M. Takigawa, M. Ichioka, and K. Machida, Eur. Phys. J. B **27**, 303 (2002).